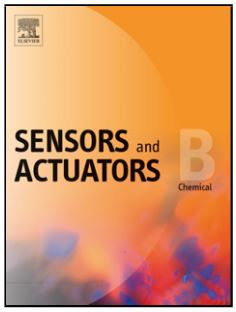

Title: Humidity-Sensing Performance of Layer-by-Layer Self-Assembled Tungsten Disulfide/Tin Dioxide Nanocomposite

Authors: Dongzhi Zhang, Yuhua Cao, Peng Li, Junfeng Wu, Xiaoqi Zong

PII: S0925-4005(18)30533-1
DOI: https://doi.org/10.1016/j.snb.2018.03.043
Reference: SNB 24328

To appear in: *Sensors and Actuators B*

Received date: 1-10-2017
Revised date: 10-2-2018
Accepted date: 11-3-2018

Please cite this article as: Dongzhi Zhang, Yuhua Cao, Peng Li, Junfeng Wu, Xiaoqi Zong, Humidity-Sensing Performance of Layer-by-Layer Self-Assembled Tungsten Disulfide/Tin Dioxide Nanocomposite, Sensors and Actuators B: Chemical https://doi.org/10.1016/j.snb.2018.03.043

Humidity-Sensing Performance of Layer-by-Layer Self-Assembled Tungsten Disulfide/Tin Dioxide Nanocomposite

Dongzhi Zhang [a,*], Yuhua Cao [a], Peng Li [b,*], Junfeng Wu [a], Xiaoqi Zong [a]

[a] College of Information and Control Engineering, China University of Petroleum (East China), Qingdao 266580, China

[b] State Key Laboratory of Precision Measurement Technology and Instruments, Department of Precision Instruments, Tsinghua University, Beijing 100084, China

*Corresponding authors: Dongzhi Zhang; Peng Li

E-mail address: dzzhang@upc.edu.cn; pengli@mail.tsinghua.edu.cn

Tel: +86-532-86981335

Fax: +86-532-86983326

Highlights

- WS_2/SnO_2 nanocomposite was fabricated by layer-by-layer (LbL) self-assembly route.
- Characterization and humidity sensing properties of WS_2/SnO_2 nanocomposite were investigated.
- The WS_2/SnO_2 sensor exhibited the unparalleled response and sensitivity toward humidity.

Abstract

In this article, we demonstrate a humidity sensor based on WS_2/SnO_2 nanocomposite via layer-by-layer (LbL) self-assembly technique on a FR4 (Flame Resistant 4) epoxy substrate with interdigital electrodes (IDEs). The component, morphology, and chemical state of WS_2/SnO_2 film was fully examined by X-ray diffraction (XRD), scanning electron microscopy (SEM), energy dispersive spectrometry (EDS), X-ray photoelectron spectroscopy (XPS) and transmission electron microscopy (TEM). The humidity sensing characteristics of WS_2/SnO_2 film sensor were investigated at room temperature. The WS_2/SnO_2 film sensor exhibited supreme sensing properties, including unprecedented response/sensitivity, rapid response rate, and good repeatability. The WS_2/SnO_2 film sensor illustrated 36 and 89 times higher responses than that of pure WS_2 and SnO_2 devices, respectively. To our knowledge, the sensor exhibited the unparalleled response and sensitivity among the existing humidity sensors ever reported. Moreover, the presented sensor demonstrated good performance in monitoring human respiration. We investigated the electrical characteristics of the WS_2/SnO_2 film by impedance spectroscopy and bode plot. The equivalent circuit model was established, and the humidity sensitive mechanism of WS_2/SnO_2 nanocomposite film was systematically investigated. The present work demonstrates that LbL self-assembled WS_2/SnO_2 nanocomposite is an excellent material candidate for the fabrication of ultrahigh-performance humidity sensor.

Keywords: WS_2/SnO_2 nanocomposite; layer-by-layer self-assembly; humidity sensing; capacitance

1. Introduction

Humidity sensing is of great importance in varying fields, such as atmospheric monitoring, industrial production, and medical care [1, 2]. Up to date, various transduction techniques have been utilized to develop humidity sensors, including capacitance [3], resistance [4], optical fiber [5], field effect transistor (FET) [6], surface acoustic wave (SAW) [7], and quartz crystal microbalance (QCM) [8]. Additionally, plenty of nano-materials such as metal oxides, graphene, and nanohybrids have been applied to fabricate humidity-sensors. They are capable of realizing rapid detection with low cost, low power consumption, and can be miniaturized for portable sensors. Tin dioxide (SnO_2), an n-type semiconducting material with band gap of 3.6 eV, exhibits the possibility of humidity sensing and excellent electrochemical stability. However, SnO_2 humidity nanosensors displayed long response/recovery time and low sensitivity [9, 10]. Therefore, many efforts have been devoted to improving humidity-sensing performance of SnO_2 humidity nanosensors. For example, semiconductor heterojunction systems were reported to enhance the sensitivity, such as graphene-SnO_2 [11], TiO_2-SnO_2 [12], WO_3-SnO_2 [13], In-SnO_2/graphitic carbon nitride (g-C_3N_4) [14] and MoS_2-SnO_2 [15].

Graphene, a two-dimensional (2D) nano-material, has been attracting significant attention due to its extraordinary electrical, optical, and mechanical properties [16]. However, zero-band gap limits its applications in sensing field. Recently, transition metal dichalcogenides (TMDs) have attracted great interest due to the existence of band-gap, outstanding electronic properties, and two-dimensional nature [17]. TMDs

are typically described by the formula MX_2, where M represents transition metal element (Mo, W, Nb, Ti, Ta) and X is chalcogenide compound (S, Se, Te). Among them, tungsten disulfide (WS_2) has been extensively studied because of its excellent hydrolytic properties as well as earth-abundance [18-20]. Bulk WS_2 is a semiconductor with indirect band gap of 1.4 eV, while monolayer WS_2 has direct band gap of 2.1 eV. Because of its excellent optical, electrical, and mechanical properties, WS_2 microsheets have been widely used for various fields including field emission [21], lubrication coatings [22], field-effect transistors [23], sensors [24, 25], photoluminescence [26-28], and solar cells [29]. The results have proved that WS_2 has great potential for gas (NH_3 [30, 32], NO_2 [31], CO [32]) and humidity detection [33]. However, the humidity sensor based on WS_2/SnO_2 heterojunction has not been reported. As such, constructing a humidity sensor which is able to realize rapid detection with low power consumption, low cost, excellent performance, and the possibility of integration still attracts considerable attention.

Here, we demonstrated a WS_2/SnO_2 nanocomposite humidity sensor via layer-by-layer (LbL) self-assembly technique on FR4 substrate with interdigital electrodes (IDEs). The component, chemical state and morphology of the WS_2/SnO_2 nanocomposite film was characterized by X-ray diffraction (XRD), scanning electron microscopy (SEM), energy dispersive spectrometry (EDS), X-ray photoelectron spectroscopy (XPS) and transmission electron microscopy (TEM). The sensing characteristics of the WS_2/SnO_2 film sensor were investigated in a wide relative humidity range, an ultrahigh response of 141260 and an unprecedented sensitivity of

55846 pF/%RH were yielded. The WS_2/SnO_2 film sensor exhibited 36 and 89 times higher responses than that of pure WS_2 and SnO_2 counterparts, respectively. The electrical characteristics of the films were investigated by impedance spectroscopy and bode plot, and the humidity sensitive mechanism of WS_2/SnO_2 nanocomposite film was revealed.

2. Experimental Section

2.1 Materials synthesis

Sodium tungstate dehydrate ($Na_2WO_4 \cdot 2H_2O$), oxalic acid ($C_2H_2O_4$), thioacetamide (TAA), tin chloride pentahydrate ($SnCl_4 \cdot 5H_2O$) and aqueous ammonia ($NH_3 \cdot H_2O$) were obtained from Sinopharm Chemical Reagent Co. Ltd. (Shanghai, China). Polycation and polyanion were 1.5 wt% poly (diallyldimethylammonium chloride) [PDDA, MW of 200−350 K, Sigma-Aldrich] and 0.3 wt% poly (sodium 4-styrenesulfonate) [PSS, MW of 70 K, Sigma-Aldrich], respectively, which were used for LbL self-assembly. 0.5 M NaCl was added into PDDA and PSS solutions to enhance ion concentration. All reagents were used without further pretreatment.

In this work, a facile hydrothermal route was utilized to synthesize WS_2 microsheets and SnO_2 microspheres. Precursors, $Na_2WO_4 \cdot 2H_2O$ (1.2 g) and TAA (1.6 g), were dissolved into 80 mL deionized (DI) water and stirred for 30 min. Sequentially, 0.6 g oxalic acid was added to the above solution to form an acid environment and stirred for 30 min. Lastly, the mixed solution was heated in a Teflon-lined autoclave at 200 °C for 24 h (hydrothermally treatment).

The synthesis of SnO_2 microsphere was similar to that of WS_2 microsheet. 8.75 g $SnCl_4 \cdot 5H_2O$ were dissolved into 20 mL of DI water and 2.5 mL of aqueous ammonia were added. Subsequently, the solution was treated by ultrasonication for 30 min in order to form homogeneous suspension. At last, the suspension was transferred into a Teflon-lined autoclave and heated at 180 °C for 12 h.

2.2 Sensor fabrication

The sensor was fabricated on a FR4 (Flame Resistant 4) epoxy substrate via a facile LbL self-assembly approach, which was described in our previous work [34]. The electrostatic interaction between the anions and cations was the nano-film driving force. After repeated alternately deposition, the multilayer alternately functional composite film were fabricated successfully. The preparation process is shown in Figure 1. Two bilayers of PDDA/PSS were sequentially deposited on the substrate with interdigital electrodes (IDEs) as adhesion layer to improve the binding force between IDEs device and upper layer, followed by alternative immersing the IDEs device into SnO_2 and WS_2 solutions for five cycles. The deposition time of polyelectrolytes (PDDA, PSS) was 10 min and 15 min for WS_2/SnO_2. The sensor was intermediate rinsed with DI water and dried with nitrogen after each monolayer assembly to strengthen the interconnection between layers. The schematic view of LbL self-assembled WS_2/SnO_2 nanocomposite film was shown in Figure 2.

2.3 Humidity measurement setup

The humidity sensing experiment was carried out at room temperature of 25ºC. We used classical saturated salt solution methods to yield different relative humidity

(RH) levels, as reported in our previous work [35]. Saturated solutions of LiCl, CH_3COOK, $MgCl_2$, K_2CO_3, $Mg(NO_3)_2$, $CuCl_2$, NaCl, KCl and K_2SO_4 in a closed vessel at 25°C provide 11%, 23%, 33%, 43%, 52%, 67%, 75%, 87% and 97%RH levels, respectively. Phosphorus pentoxide powder (P_2O_5) was used as a desiccant, which yielded 0% RH for the sensor recovery. TH2828 precision LCR meter was applied to record the capacitance variations and complex impedance spectroscopy of the WS_2/SnO_2 film sensor during humidity sensing. The capacitance of the sensor as a function of RH was measured by exposing the sensor inside the closed vessels with different RH levels for the uptake of water molecules. Normalized response C and sensitivity S are used to evaluate the performance of WS_2/SnO_2 film sensors, which are defined by $C=C_x/C_0$ and $S=\Delta C/\Delta RH$ respectively, where C_x and C_0 are the capacitance of the sensor at x% and 0% RH, respectively, ΔC is the change in capacitance, and ΔRH is the RH change.

3. Results and discussion

3.1 Structure characterization

The XRD analysis of WS_2, SnO_2 and WS_2/SnO_2 samples was carried out by an X-ray diffractometer (Rigaku D/Max 2500PC) using Cu Kα radiation (λ=1.5418Å). All the synthesized samples were examined with diffraction peaks in the range of 20°-80° as illustrated in Figure 3. The diffraction peaks of SnO_2 sample are observed at 2θ of 26.41°, 33.82°, 37.60°, 51.71° and 65.68°, which correspond to the (110), (101), (200), (211), and (301) planes of the rutile SnO_2 respectively (JCPDS Card no. 41-1445). The result indicates the successfully synthesis of SnO_2 [36, 37]. The XRD

spectrum of WS_2 agrees well with the hexagonal structure (JCPDS No: 87-2417) without impurity peaks [38]. The diffraction peaks of WS_2 are located at 2θ of 29.20°, 33.15°, 33.88°, 40.02°, 44.37°, 50.07°, 58.69°, 60.36°, 66.79° and 76.24°, which correspond to (004), (100), (101), (103), (006), (105), (110), (112), (108) and (116) planes, respectively. The XRD pattern of LbL self-assembled WS_2/SnO_2 nanocomposite demonstrates the main characteristic peaks of the both WS_2 and SnO_2, confirming the existence of WS_2 and SnO_2.

The elements composition of the WS_2/SnO_2 nanocomposite was analyzed by Hitachi S-4800 equipped with an energy dispersive spectrometer (EDS). As demonstrated in Figure 4 (a), only W, S, Sn and O peaks are detected [45, 46]. X-ray photoelectron spectroscopy (XPS, Thermo Scientific instrument) was applied to inspect the surface composition and chemical state of the WS_2/SnO_2 nanocomposite. The XPS survey spectrum is shown in Figure 4 (b), which also confirms that the main constituent elements were W, S, Sn and O. Figure 4 (c) clearly shows that W atom in the sample has two different valence states, W^{4+} and W^{6+}. The major peaks of W^{4+} at 32.38 and 34.53 eV are correspond to W^{4+} $4f_{7/2}$ and W^{4+} $4f_{5/2}$, respectively. Moreover, W^{6+} also has two major peaks at 35.43 and 37.98 eV, which are attributed to the W^{6+} $4f_{7/2}$ and W^{6+} $4f_{5/2}$, respectively [41-43]. The spectra of S 2p shown in Figure 4 (d) exhibit two main peaks at 161.88 and 163.28 eV, which corresponding to S^{2-} $2p_{3/2}$ and S^{2-} $2p_{1/2}$. Figure 4 (e) shows that two peaks at 494.44 and 486.03 eV, which are ascribed to the doublet Sn $3d_{3/2}$ and Sn $3d_{5/2}$ of Sn from SnO_2. The XPS spectrum of O 1s in Figure 4 (f), displaying two major peaks at 529.78 and 532.08eV in

correspondence with the oxygen in SnO_2 [44, 45].

Field emission scanning electron microscopy (FESEM; Hitachi S-4800, Japan) was used to identify the morphology of WS_2, SnO_2, and LbL self-assembled WS_2/SnO_2 nanocomposite. Figure 5 (a) and (b) show the hexagon shaped WS_2 [46] and SnO_2 microspheres [36]. Figure 5 (c) demonstrates the combination of SnO_2 microspheres and hexagon shaped WS_2. Figure 5 (d) illustrates the cross-sectional image of WS_2/SnO_2 sample, which confirms the sensing film has clearly laminated and pronouns nanostructure.

The nanostructure of the as-prepared samples was further investigated by transmission electron microscope (TEM; JEOL JEM-2100, Japan). Figures 6 (a), (b) are the TEM images of WS_2 and WS_2/SnO_2 nanocomposite, respectively, Figures. 6 (c), (d) are high-resolution TEM (HRTEM) image which can reveal the lattice fringes of WS_2 and SnO_2, respectively. Figure 6 (c) shows SnO_2 microspheres on WS_2 microsheets with labeled lattice fringes. The lattice fringe spacing of 0.305 nm is attributed to the (004) plane of WS_2. And the measured spacing between adjacent lattice fringes are 0.334 nm, corresponding to the (110) plane of the SnO_2 [14]. Figure 6 (d) is the TEM image of WS_2 microsheets with neighboring fringe spacing of 0.273 nm and 0.226 nm, which are attributed to the (100) and (103) planes of WS_2 [47, 48].

3.2. Humidity-sensing performance

Figure 7 demonstrates the capacitance of the WS_2/SnO_2 film sensor versus various RH at different operation frequencies of 500, 1k, 10k and 10M Hz, respectively. The capacitance of the WS_2/SnO_2 film sensor increases dramatically

with the raising of RH. This is due to the absorbed water molecules are beneficial to enhance the polarization effect and increase the dielectric constant of the film, leading to the increase of film capacitance [49]. The capacitance shows the maximum capacitance variation at 500 Hz among the four frequencies, this is because the space-charge polarization of adsorbed water occurs in the film is hard to keep up the electrical field direction at higher frequencies [50]. Nevertheless, the capacitive reactance of the sensor is much larger at excessive low frequencies, which will degrade the measuring precision and working stability. Thereby, 500 Hz was chosen for subsequent humidity sensing experiments in order to achieve better sensitivity.

We compared the humidity-sensing responses of WS_2, SnO_2, and WS_2/SnO_2 nanocomposite. The three types of sensors were tested under the same experimental conditions over a wide RH range of 11%-97% RH. Figure 8 (a) shows the comparative results of WS_2/SnO_2 film sensor with pure WS_2 and SnO_2 counterparts, the response values measured at 97% RH are about 6682, 2687 and 141260 for WS_2, SnO_2, and WS_2/SnO_2 sensor, respectively, indicating the WS_2/SnO_2 film sensor has the highest response. Figure 8 (b) shows the response of the WS_2/SnO_2 film sensor as a function of RH. The fitting equation is $Y = 214.38\ e^{X/13.78} - 3467.50$ for the sensor response toward 11-97%RH, where Y is the sensor response, and X is RH. The regression coefficient, R^2, is 0.9971.

We performed a switching experiment in RH levels of 11-97%RH to explore the humidity-sensitive response characteristics of LbL self-assembled WS_2/SnO_2 film sensor. The time-dependent capacitance measurement toward switching RH for the

WS_2/SnO_2 film sensor is shown in Figure 9 (a). The time interval for response/recovery duration was 100 s. The sensor capacitance increases by approximately 5 orders of magnitude from 34 pF to 4802.83 nF toward RH varies from 11% to 97% RH, and an ultrahigh sensitivity of 55846 pF/%RH was obtained. Figure 9 (b) shows the capacitance response of the WS_2/SnO_2 film sensor toward step increases of RH and then recovery. The graph clearly indicates that the capacitance monotonically increased with the step increase of RH. It can be observed that the sensor is recovered to the initiate resistance rapidly when the sensor is exposed to dry air. Figure 9 (c) illustrates the repeatability of the WS_2/SnO_2 film sensor upon exposure to 23%, 52% and 85% RH from dry air (5 cycles for each RH). Good repeatability can be observed and the equilibrium-state capacitances were 64 pF (23% RH), 58816 pF (52% RH), and 2049231 pF (85% RH), respectively. Figure 9 (d) demonstrates the long-term stability of WS_2/SnO_2 film sensor in 23%, 52%, 85% and 97% RH, respectively. The capacitance values of the WS_2/SnO_2 film sensor remained stable within 30 days, suggesting excellent stability.

Hysteresis is an important characteristic of humidity sensors. We further investigated the hysteresis characteristics of WS_2/SnO_2 film sensor. The measurement was firstly switched from low RH to high RH, and then conversely from high RH to low RH. Each exposure/recovery cycle was carried out through an exposure interval of 100 s, followed by a recovery interval of 100 s in dry air as shown in Figure 10 (a). The hysteresis error (H_e) can be expressed as: $H_e = \pm \Delta H_{max}/2F_{FS}$, where ΔH_{max} is the difference between the response of humidity sensor toward the same RH value during

adsorption and desorption process, and F_{FS} is the full scale output [51]. It is noteworthy that the maximum H_e is less than 1.9% (at 75% RH) as shown in Figure 10 (b), indicating low hysteresis and good reliability of the WS_2/SnO_2 film sensor.

We demonstrated a potential application (respiratory monitoring) using the WS_2/SnO_2 film humidity sensor. The sensor was placed approximately 4-5 cm away from nose. Figure 11 displays the response of the sensor during human respiration monitoring. It shows a periodic capacitance changes which frequency is identical to the respiration. The breath response characteristic for a normal adult was measured in 100 s, and 28 repetitive cycles for breathing were observed. The capacitance response showed sharp rise during exhaling and fall while inhaling corresponding to the breathing cycles. We believe this device provides a good platform for space suits, anti-asphyxia, respiratory detection and health care.

Table 1 clearly demonstrates the humidity sensing properties of our WS_2/SnO_2 film sensor compared with the previous works [11, 52-57]. The comparison is made over the state-of-the-art sensors made from 2D materials (i.e., graphene, MoS_2, WS_2) via LbL self-assembly, solution dripping, sulfurization, liquid exfoliation and hydrothermal methods. To our knowledge, our WS_2/SnO_2 film sensor yielded the highest response and highest sensitivity over the existing humidity sensors ever reported, highlighting the unique advantages of WS_2/SnO_2 film as an ideal candidate for building humidity sensors.

3.3. Humidity sensing mechanism

WS_2/SnO_2 nanocomposite is sensitive to water molecules, which is attributed to

the synergistic effect of WS_2 and SnO_2. Figure 12 (a) illustrates the adsorption mechanism of water molecules on WS_2/SnO_2 nanocomposite. Firstly, a small amount of water molecules are chemisorbed, and then some water molecules are physisorbed as RH increases. The chemisorbed water molecules are discontinuous and unable to move freely because they are restricted onto the film surface by double hydrogen bonding. As the RH further increased, much more water molecules are physisorbed, and the water molecules turn to be active and exhibit liquid-like behavior. The proton-hopping occurs according to the Grothuss chain reaction ($H_2O + H_3O^+ \leftrightarrows H_3O^+ + H_2O$) [58, 59].

The nanostructure of WS_2/SnO_2 nanohybrid contributes to the enhanced humidity sensing properties. The incorporation of SnO_2 into WS_2 nanosheets brings more active sites such as oxygen vacancies and defects, which can provide high surface exposure for adsorption of water molecules. WS_2 nanosheets possess natural band gap, low resistivity and high carrier mobility, serving as direct conduction paths for the electrons transfer in the SnO_2 nanospheres. Furthermore, the n-n heterojunction created at the interfaces of n-typeWS_2 microsheets and n-type SnO_2 nanospheres may be another major contribution to the enhanced response for the WS_2/SnO_2 film sensor. Figure 12 (b) shows energy-band diagram of WS_2/SnO_2 film. The work functions for WS_2 and SnO_2 are W_1=4.6 eV and W_2=4.52 eV, respectively. There is an energy barrier ($\triangle E_B=W_1-W_2$) generated at the interface between WS_2 and SnO_2 [60]. When the sensor is under humidity environment, the adsorbed water molecules react with the surface of WS_2/SnO_2 nanocomposite and release a quantity

of electrons. The injected electrons can increase the concentration of the electron carriers in WS_2/SnO_2 film, leading to the decrease of the barrier height and the increase of the conduction [61]. Therefore, the response of WS_2/SnO_2 film sensor is significantly increased as compared to that of the pristine WS_2 and SnO_2.

To confirm the humidity-sensing mechanisms of the WS_2/SnO_2 film at various RH levels, the complex impedance spectroscopy (CIS) combining with Bode plots was applied. Figure 13 shows the complex impedance spectra, equivalent circuits and corresponding Bode plots of WS_2/SnO_2 film at different RH. The operation frequency changed from 500 Hz to 1M Hz with RH range from 11% to 97%. At low RH (11%), the CIS curve plotted in Figure 13 (a) is a straight line, the equivalent circuit could be described by a constant phase element (CPE), and its corresponding Bode diagram is shown in Figure 13 (d). The impedance value of WS_2/SnO_2 film is linearly related to the frequency in the logarithmic coordinate system, and the impedance angle is almost constant, approximately -90º. In this case, only a small amount of molecules are adsorbed onto the WS_2/SnO_2 film, the ion transfer is difficult to be realized due to the fact that the film surface is not completely water-covered.

Figure 13 (b) shows the CIS curve at medium RH (52% RH), and a semicircle is observed, attributing to the intrinsic impedance of WS_2/SnO_2 film [62]. The equivalent circuit can be modeled by a resistor and capacitor in parallel [63-65]. The impedance value decreases with the increase of operating frequency, and the impedance angle changes from 0º to -90º, as shown in Figure 13 (e). At this stage, excess water molecules are adsorbed to form hydronium ions. The proton hopping

occurs and leads to the impedance of WS_2/SnO_2 film decreases with increasing RH.

With the RH further increases (85% RH), a short straight line appears after the semicircle at low frequency region as shown in Figure 13 (c). Warburg impedance is introduced to the equivalent circuit, accounting for the diffusion process of ions or charge carriers at the WS_2/SnO_2 film/electrode interface [66]. The impedance angle of WS_2/SnO_2 film is almost no significantly variation with the increasing of working frequency, as shown in Figure 13 (f). At this stage, the serial water layer exhibits liquid-like behavior and further accelerates the proton transfer, which results in a significant decrease in sensor impedance and a sharp increase in sensor capacitance.

4. Conclusions

A humidity sensor based on WS_2/SnO_2 nanocomposite was presented in this paper, which was realized by LbL self-assembly technique. The component, structure, chemical state and morphology of the as-prepared film were characterized by XRD, SEM, EDS, XPS and TEM. The capacitive sensing properties of WS_2/SnO_2 film sensor were measured against humidity at room temperature. The LbL self-assembled WS_2/SnO_2 film sensor exhibits excellent sensing properties, which far surpasses that of pure WS_2 and pure SnO_2. Moreover, the humidity sensing characteristics of the WS_2/SnO_2 film sensor were further investigated by impedance spectroscopy and bode plot. The LbL self-assembled WS_2/SnO_2 nanocomposite was proved to be an excellent building block for ultrahigh-performance humidity sensor toward various applications.

Acknowledgements

This work was supported by the National Natural Science Foundation of China (51777215, 51405257), the Fundamental Research Funds for the Central Universities of China (18CX07010A), the Open Fund of National Engineering Laboratory for Mobile Source Emission Control Technology (NELMS2017B03), and the Science and Technology Development Plan Project of Qingdao (16-6-2-53-nsh).

References

[1] Z. Wei, Z. Zhou, Q. Li, J. Xue, A. D. Falco, Z. Yang, J. Zhou, X. Wang, Flexible nanowire cluster as a wearable colorimetric humidity sensor, Small 13 (2017) 1700109.

[2] U. Mogera, A.A. Sagade, S. J. George, G. U. Kulkarni. Ultrafast response humidity sensor using supramolecular nanofibre and its application in monitoring breath humidity and flow, Sci. Rep. 4 (2014) 4103.

[3] K. Narimani, F.D. Nayeri, M. Kolahdouz, P. Ebrahimi, Fabrication, modeling and simulation of high sensitivity capacitive humidity sensors based on ZnO nanorods Sens. Actuators B 224 (2016) 338-343.

[4] K.-J. Park, M.-S. Gong, A water durable resistive humidity sensor based on rigid sulfonated polybenzimidazole and their properties, Sens. Actuators B 246 (2017) 53-60.

[5] H. Guan, K. Xia, C. Chen, Y. Luo, J. Tang, H. Lu, J. Yu, J. Zhang, Y. Zhong, Z. Chen, Tungsten disulfide wrapped on micro fiber for enhanced humidity sensing, Opt. Mater. Express 7 (2017) 1686-1696.

[6] J. Miao, L.Cai, S. Zhang, J. Nah, J. Yeom, C. Wang, Air-stable humidity sensor using few-layer black phosphorus, ACS Appl. Mater. Interfaces 9 (2017) 10019-10026.

[7] R. Rimeika, D. Čiplys, V. Poderys, R. Rotomskis, M.S. Shur, Fast-response and low-loss surface acoustic wave humidity sensor based on bovine serum albumin-gold nanoclusters film, Sens. Actuators B 239 (2017) 352-357.

[8] Y. Yao, H. Zhang, J. Sun, W. Ma, L. Li, W. Li, J. Du, Novel QCM humidity sensors using stacked black phosphorus nanosheets as sensing film, Sens. Actuators B 244 (2017) 259-264.

[9] Q. Kuang, C.S. Lao, Z.L. Wang, Z.X. Xie, L.S. Zheng. High-sensitivity humidity sensor based on a single SnO_2 nanowire, J. Am. Chem. Soc. 129 (2007) 6070-6071.

[10] M. Parthibavarman, V. Hariharan, C. Sekar. High-sensitivity humidity sensor based on SnO_2 nanoparticles synthesized by microwave irradiation method, Mater. Sci. Eng. C 31 (2011) 840-844.

[11] D. Zhang, H. Chang, P. Li, R. Liu, Q. Xue. Fabrication and characterization of an ultrasensitive humidity sensor based on metal oxide/graphene hybrid nanocomposite, Sens. Actuators B 225 (2016) 233-240.

[12] Z.L. Yang, Z.Y. Zhang, K.C. Liu, Q. Yuan, B. Dong. Controllable assembly of SnO_2 nanocubes onto TiO_2 electrospun nanofibers toward humidity sensing applications, J. Mater. Chem. C 3 (2015) 6701-6708.

[13] H. Li, B. Liu, D.P. Cai, Y.R. Wang, Y. Liu, L. Mei, L.L. Wang, D.D. Wang, Q.H. Li, T.H. Wang. High-temperature humidity sensors based on WO_3-SnO_2 composite hollow nanospheres, J. Mater. Chem. A 2 (2014) 6854-6862.

[14] R. Malik, V.K. Tomer, V. Chaudhary, M.S. Dahiya, A. Sharma, S.P. Nehra, S. Duhan, K. Kailasam, An excellent humidity sensor based on In-SnO_2 loaded mesoporous graphitic carbon nitride, J. Mater. Chem. A 5 (2017) 14134-14143.

[15] D. Zhang, Y. Sun, P. Li, Y. Zhang. Facile fabrication of MoS_2-modified SnO_2 hybrid nanocomposite for ultrasensitive humidity sensing, ACS Appl. Mater. Interfaces 8 (2016) 1442-449.

[16] A.K. Geim. Graphene: status and prospects, Science 324 (2009) 1530-1534.

[17] B. Li, J. Wang, H. Zou, S. Garaj, C.T. Lim, J. Xie, N. Li, D.T. Leong, Low-dimensional transition metal dichalcogenide nanostructures based sensors, Adv. Funct. Mater. 26 (2016) 7034-7056.

[18] H.I. Karunadasa, E. Montalvo, Y. Sun, M. Majda, J.R. Long, C.J. Chang. A molecular MoS_2 edge site mimic for catalytic hydrogen generation, Science 335 (2012) 698-702.

[19] K. Kang, K. Godin, Y.D. Kim, S. Fu, W. Cha, J. Hone, E.H. Yang, Graphene-assisted antioxidation of tungsten disulfide monolayers: substrate and electric-field effect, Adv. Mater. 29 (2017) 1603898.

[20] C.E. Giusca, I. Rungger, V. Panchal, C. Melios, Z. Lin, Y. Lin, E. Kahn, A.L. Elías, J.A. Robinson, M. Terrones, O. Kazakova, Excitonic effects in tungsten disulfide monolayers on two-layer graphene, ACS Nano 10 (2016) 7840-7846.

[21] G. Wang, C. Robert, M.M. Glazov, F. Cadiz, E. Courtade, T. Amand, D. Lagarde, T. Taniguchi, K. Watanabe, B. Urbaszek, X. Marie, In-plane propagation of light in transition metal dichalcogenide monolayers: optical selection rules, Phys. Rev. Lett. 119 (2017) 47401.

[22] Y. Lian, J. Deng, S. Li, G. Yan, S. Lei, Friction and wear behavior of WS_2/Zr self-lubricating soft coatings in dry sliding against 40Cr-hardened steel balls, Tribol. Lett. 53 (2014) 237-246.

[23] X. Liu, J. Hu, C. Yue, N.D. Fera, Y. Ling, Z. Mao, J. Wei, High performance field-effect transistor based on multilayer tungsten disulfide, ACS Nano 8 (2014) 10396-10402.

[24] A.S. Pawbake, R.G. Waykar, D.J. Late, S.R. Jadkar, Highly transparent wafer-scale synthesis of crystalline WS_2 nanoparticle thin film for photodetector and humidity-sensing applications, ACS Appl. Mater. Interfaces 8 (2016) 3359-3365.

[25] Y. Luo, C. Chen, K. Xia, S. Peng, H. Guan, J. Tang, H. Lu, J. Yu, J. Zhang, Y. Xiao, Z. Chen, Tungsten disulfide (WS_2) based all-fiber-optic humidity sensor, Opt. Express 24 (2016) 8956-8966.

[26] Y. Sheng, X. Wang, K. Fujisawa, S. Ying, A.L. Elias, Z. Lin, W. Xu, Y. Zhou, A.M. Korsunsky, H. Bhaskaran, M. Terrones, J.H. Warner, Photoluminescence segmentation within individual hexagonal monolayer tungsten disulfide domains grown by chemical vapor deposition, ACS Appl. Mater. Interfaces 9 (2017) 15005-15014.

[27] Z. He, Y. Sheng, Y. Rong, G.-D. Lee, J. Li, J.H. Warner, Layer-dependent modulation of tungsten disulfide photoluminescence by lateral electric fields, ACS Nano 9 (2015) 2740-2748.

[28] Y. Yu, Y. Zhang, X. Song, H. Zhang, M. Cao, Y. Che, H. Dai, J. Yang, H. Zhang, J. Yao, PbS-decorated WS_2 phototransistors with fast response, ACS Photonics 4 (2017) 950-956.

[29] S.H. Ahn, A. Manthiram, Edge-oriented tungsten disulfide catalyst produced from mesoporous WO_3 for highly efficient dye-sensitized solar cells, Adv. Energy Mater. 6 (2016) 1501814.

[30] X. Li, X. Li, Z. Li, J. Wang, J. Zhang, WS_2 nanoflakes based selective ammonia sensors at room temperature, Sen. Actuators B 240 (2017) 273-277.

[31] F. Perrozzi, S.M. Emamjomeh, V. Paolucci, G. Taglieri, L. Ottaviano, C. Cantalini, Thermal stability of WS_2 flakes and gas sensing properties of WS_2/WO_3 composite to H_2, NH_3 and NO_2, Sen. Actuators B 243 (2017) 812-822.

[32] C. Zhou, W. Yang, H. Zhu, Mechanism of charge transfer and its impacts on Fermi-level pinning for gas molecules adsorbed on monolayer WS_2, J. Chem. Phys. 142 (2015) 214704.

[33] A.S. Pawbake, R.G. Waykar, D.J. Late, S.R. Jadkar, Highly transparent wafer-scale synthesis of crystalline WS_2 nanoparticle thin film for photodetector and humidity-sensing applications, ACS Appl. Mater. Interfaces 8 (2016) 3359-3365.

[34] D. Zhang, J. Tong, B. Xia. Humidity-sensing properties of chemically reduced graphene oxide/polymer nanocomposite film sensor based on layer-by-layer nano self-assembly, Sen. Actuators B 197 (2014) 66-72.

[35] D. Zhang, C. Jiang, Y. Sun, Q. Zhou. Layer-by-layer self-assembly of tricobalt tetroxide-polymer nanocomposite toward high-performance humidity-sensing, J. Alloys Compd. 711 (2017) 652-658.

[36] D. Zhang, J. Liu, H. Chang, A. Liu, B. Xia. Characterization of a hybrid composite of SnO_2 nanocrystal-decorated reduced graphene oxide for ppm-level ethanol gas sensing application, RSC. Adv. 5 (2015) 18666.

[37] B. Babu, A.N. Kadam, R.V.S.S.N. Ravikumar, C. Byon. Enhanced visible light photocatalytic activity of Cu-doped SnO_2 quantum dots by solution combustion synthesis, J. Alloys Compd. 703 (2017) 330-336.

[38] S.V. Prabhakar Vattikuti, Chan Byon, Veerendra Chitturi. Selective hydrothermally synthesis of hexagonal WS_2 platelets and their photocatalytic performance under visible light irradiation, Superlattices Microstruct. 94 (2016) 39-50.

[39] Z.Y. Wang, C. Zhao, T.Y. Han, Y. Zhang, S. Liu, T. Fei, G.Y. Lu, T. Zhang. High-performance reduced graphene oxide-based room-temperature NO_2 sensors: A combined surface modification of SnO_2 nanoparticles and nitrogen doping approach, Sens. Actuators B 242 (2017) 269–279.

[40] X.H. Zhang, H.X. Xu, J.T. Wang, X. Ye, W.N. Lei, M.Q. Xue, H. Tang, C.S. Li. Synthesis of ultrathin WS_2 nanosheets and their tribological properties as lubricant additives, Nanoscale Res, Lett. 11 (2016) 442.

[41] D. Zhang, C. Jiang, P. Li, Y. Sun. Layer-by-layer self-assembly of Co_3O_4 nanorod-decorated MoS_2 nanosheet-based nanocomposite toward

high-performance ammonia detection, ACS Appl. Mater. Interfaces 9 (2017) 6462-6471.

[42] Y.C. Wu, A.M. Liu, J.T. Chen, X.J. Cai, P. Na. Hydrothermal fabrication of hyacinth flower-like WS_2 nanorods and their photocatalytic properties, Mater. Lett. 189 (2017) 282-2855.

[43] T. Alphazan, A. Bonduelle-Skrzypczak, C. Legens, A.S. Gay, Z. Boudene, M. Girleanu, O. Ersen, C. Coperet, P. Raybaud. Highly active nonpromoted hydrotreating catalysts through the controlled growth of a supported hexagonal WS_2 phase, ACS Catal. 4 (2014) 4320-4331.

[44] Y.L. Wang, C. Liu, L. Wang, J. Liu, B. Zhang, Y. Gao, P. Sun, Y.F. Sun, T. Zhang, G.Y. Lu. Horseshoe-shaped SnO_2 with annulus-like mesoporous for ethanol gas sensing application, Sens. Actuators B 240 (2017) 1321-1329.

[45] G.Z. Wang, J.M. Feng, L. Dong, X.F. Li, D.J. Li. SnO_2 particles anchored on N-doped graphene surface as sodium-ion battery anode with enhanced electrochemical capability, Appl. Surf. Sci. 396 (2017) 269-277.

[46] H.Y. Jeong, Y.J. Jin, S.J. Yun, J. Zhao, J. Baik, D. H. Keum, H.S. Lee, Y. H. Lee. Heterogeneous defect domains in single-crystalline hexagonal WS_2, Adv. Mater. 29 (2017) 1605043.

[47] X. Shang, J.Q. Chi, S.S. Lu, J.X. Gou, B. Dong, X. Li, Y.R. Liu, K.L. Yan, Y.M. Chai, C.G. Liu. Carbon fiber cloth supported interwoven WS_2 nanosplates with highly enhanced performances for supercapacitors, Appl. Surf. Sci. 392 (2017) 708-714.

[48] H.T. Zhao, R.R. Sun, X.Y. Li, X. Sun. Enhanced photocatalytic activity for hydrogen evolution from water by $Zn_{0.5}Cd_{0.5}S/WS_2$ heterostructure, Mater. Sci. Semicond. Process. 59 (2017) 68-75.

[49] B.H. Cheng, B.X. Tian, C.C. Xiao, Y.H. Xiao, S.J. Lei. Highly sensitive humidity sensor based on amorphous Al_2O_3 nanotubes. J. Mater. Chem. 21 (2011) 1907-1912.

[50] S. Pokhrel, K.S. Nagaraja. Electrical and humidity sensing properties of chromium (III) oxide-tungsten (VI) oxide composites. Sens. Actuators B 92 (2003) 144-150.

[51] V.K. Tomer, N. Thangaray, S. Gahlot, K. Kailasam. Cubic mesoporous Ag @ CN: a high performance humidity sensor, Nanoscale 8 (2016) 19794.

[52] H.C. Bi, K.B. Yin, X. Xie, J. Ji, S. Wan, L. Sun, M. Terrones, M.S. Dresselhaus. Ultrahigh humidity sensitivity of graphene oxide, Sci. Rep. 3 (2013) 2714.

[53] H. Guo, C. Lan, Z. Zhou, P. Sun, D. Wei, C. Li, Transparent, flexible, and stretchable WS_2 based humidity sensors for electronic skin, Nanoscale 9 (2017) 6246-6253.

[54] R.K. Jha, P.K. Guha, Liquid exfoliated pristine WS_2 nanosheets for ultrasensitive and highly stable chemiresistive humidity sensors, Nanotechnol. 27 (2016) 475503.

[55] Y. Tan, K. Yu, T. Yang, Q. Zhang, W. Cong, H. Yin, Z. Zhang, Y. Chen, Z. Zhu, The combinations of hollow MoS_2 micro@nano-spheres: One-step synthesis,

excellent photocatalytic and humidity sensing properties, J. Mater. Chem. C 2 (2014) 5422-5430.

[56] D. Zhang, J. Tong, B. Xia, Q. Xue. Ultrahigh performance humidity sensor based on layer-by-layerself-assembly of graphene oxide/polyelectrolyte nanocomposite film, Sens. Actuators B 203 (2014) 263-270.

[57] N. Li, X.D. Chen, X.P. Chen, X. Ding, X. Zhao, Ultra-high sensitivity humidity sensor based on MoS_2/Ag composite films, IEEE Electr. Dev. Lett. 38 (2017) 806-809.

[58] N. Agmon, The Grotthuss mechanism, Chem. Phys. Lett. 244 (1995) 456–462.

[59] D. Zhang, J. Liu, B. Xia. Layer-by-Layer Self-assembly of zinc oxide/graphene oxide hybrid toward ultrasensitive humidity sensing, IEEE Electron Dev. Lett. 37 (2016) 916-919.

[60] D. Zhang, C. Jiang, Y. Sun. Room-temperature high-performance ammonia gas sensor based on layer-by-layer self-assembled molybdenum disulfide/zinc oxide nanocomposite film, J. Alloys Compd. 698 (2017) 476-483.

[61] N. Li, X.D. Chen, X.P. Chen, X. Ding, X. Zhao. Ultrahigh humidity sensitivity of graphene oxide combined with Ag nanoparticles, RSC Adv. 7 (2017) 45988.

[62] S. Thakur, P. Patil, Rapid synthesis of cerium oxide nanoparticles with superior humidity-sensing performance, Sens. Actuators B 194 (2014) 260-268.

[63] W.C. Geng, Q. Yuan, X.M. Jiang, J.C. Tu, L.B. Duan, J.W. Gu, Q.Y. Zhang. Humidity sensing mechanism of mesoporous MgO/KCl-SiO_2 composites

analyzed by complex impedance spectra and bode diagrams, Sens. Actuators B 174 (2012) 513-520.

[64] X.F. Song, Q. Qi, T. Zhang, C. Wang. A humidity sensor based on KCl-doped SnO_2 nanofibers, Sens. Actuators B 138 (2009) 368-373.

[65] T. Fei, K. Jiang, S. Liu, T. Zhang. Humidity sensors based on Li-loaded nanoporous polymers, Sens. Actuators B 190 (2014) 523-528.

[66] K. Jiang, T. Fei, T. Zhang, Humidity sensor using a Li-loaded microporous organic polymer assembled by 1, 3, 5-trihydroxybenzene and terephthalic aldehyde, RSC Adv. 4 (2014) 28451-28455.

Biographies

Dongzhi Zhang received his B.S. degree from Shandong University of Technology in 2004, M.S. degree from China University of Petroleum in 2007, and obtained Ph.D. degree from South China University of Technology in 2011. He is currently an associate professor at China University of Petroleum (East China), Qingdao, China. His fields of interests are gas and humidity sensing materials, nanotechnology, and polymer electronics.

Yuhua Cao received her B.S. degree in automation from Harbin University of Science and Technology in 2016. Currently, she is a graduate student at China University of Petroleum (East China), Qingdao, China. Her fields of interests include 2D nanomaterials-based sensors, precision measurement technology and instruments.

Peng Li received B.S. degree in Electronic Engineering from Tianjin University, China, in 2007, and Ph. D. degree in Precision Instruments from Tsinghua University, China, in 2012. He is currently working in Department of Mechanical engineering at Tsinghua University. His current research interests include graphene material synthesis, and graphene NEMS device fabrication and their application in actuators and sensors.

Junfeng Wu received her B.S. degree from China University of Petroleum (East China) in 2016. Currently, he is a graduate student at China University of Petroleum (East China), Qingdao, China. His fields of interests include transition-metal dichalcogenides (TMDCs)-based gas sensors.

Xiaoqi Zong received her B.S. degree from China University of Petroleum (East China) in 2016. Currently, she is graduate student at China University of Petroleum (East China), Qingdao, China. Her fields of interests include nanomaterials-based humidity and gas sensors, precision measurement technology.

Figure captions

Figure 1. LbL fabrication process of WS_2/SnO_2 nanocomposite film.

Figure 2. Sketch of LbL self-assembled WS_2/SnO_2 nanocomposite sensor.

Figure 3. XRD of WS_2, SnO_2, and WS_2/SnO_2 samples.

Figure 4. (a) EDS for WS_2/SnO_2 nanocomposite. XPS spectra of WS_2/SnO_2 sample: (b) survey spectrum, (c) W spectrum of WS_2/SnO_2 sample, (d) S spectrum of WS_2/SnO_2 sample, (e) Sn spectrum of WS_2/SnO_2 sample, and (f) O spectrum of WS_2/SnO_2 sample.

Figure 5. SEM images of (a) hexagonal WS_2 sample, (b) SnO_2 sample and (c) WS_2/SnO_2 nanocomposite, (d) cross-sectional images of WS_2/SnO_2 film.

Figure 6. TEM images of (a) WS_2 microsheets and (b) WS_2/SnO_2 nanocomposite. HRTEM images of (c) WS_2/SnO_2 nanocomposite and (d) WS_2 microsheets.

Figure 7. The capacitance of WS_2/SnO_2 film sensor exposed to various RH levels with different operation frequencies.

Figure 8. (a) Comparative results of WS_2/SnO_2 film sensor in sensing response with pure WS_2, and pure SnO_2 film. (b) The response of WS_2/SnO_2 film sensor as a function of RH in the range of 11−97%. Inset: the sensor response toward 11−67% RH.

Figure 9. Sensing characteristics of LbL self-assembled WS_2/SnO_2 film sensor. (a) Time-dependent capacitance measurement toward switching RH. (b) Capacitance response toward step increases of RH and then recovery. (c) Repeatability

performance exposed to 23%, 52%, and 85%RH. (d) Long-term stability exposed to 23%, 52%, 85% and 97%RH.

Figure 10. (a) The response and recovery characteristics under humidity cycling of absorption and desorption toward different RH. (b) Hysteresis loop characteristics of the WS_2/SnO_2 film sensor. Inset: hysteresis under different RH.

Figure 11. Capacitance response of the sensor toward human respiration.

Figure 12. (a) Schematic of humidity sensing at WS_2/SnO_2 nanocomposite film. (b) Energy-band diagram of WS_2/SnO_2 film (E_0, vacuum-energy level; W, work function; E_g, energy band gap; E_F, Fermi level; E_C, conduction band; E_V, valence band).

Figure 13. Complex impedance spectra, equivalent circuits (a, b, c) and corresponding Bode plots (d, e, f) of WS_2/SnO_2 film at different RH: (a and d) 11% RH, (b and e) 52% RH, and (c and f) 85% RH.

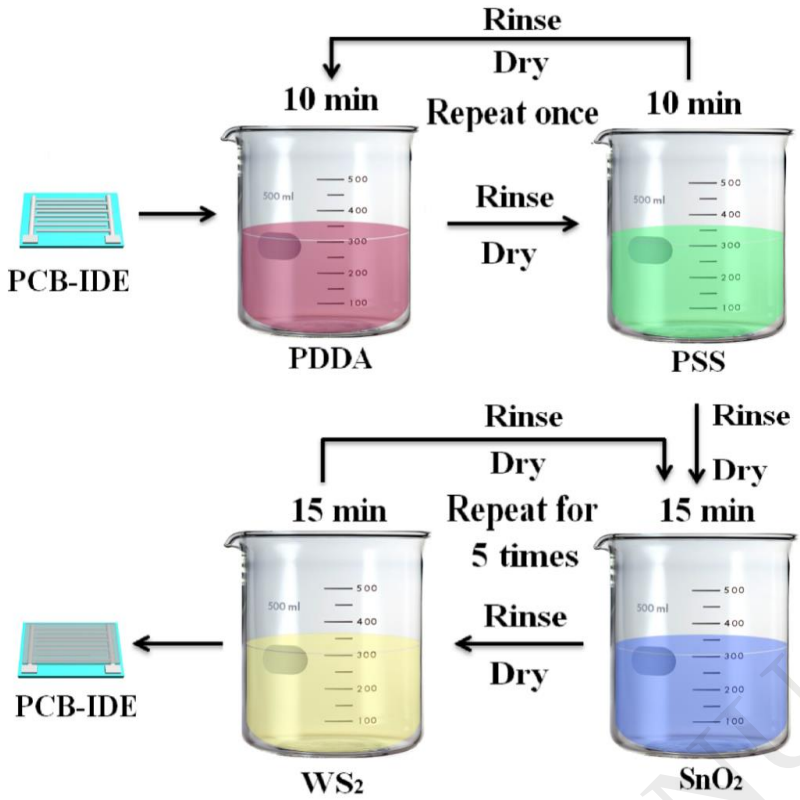

Figure 1. LbL fabrication process of WS_2/SnO_2 nanocomposite film.

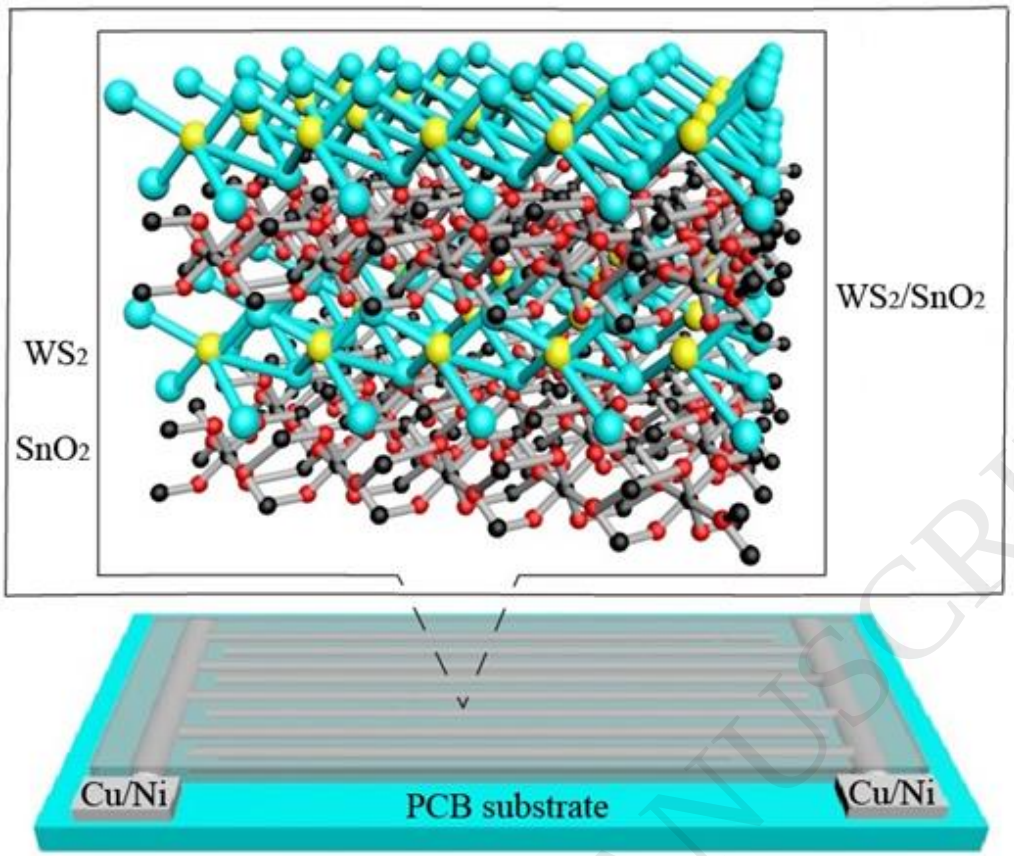

Figure 2. Sketch of LbL self-assembled WS_2/SnO_2 nanocomposite sensor.

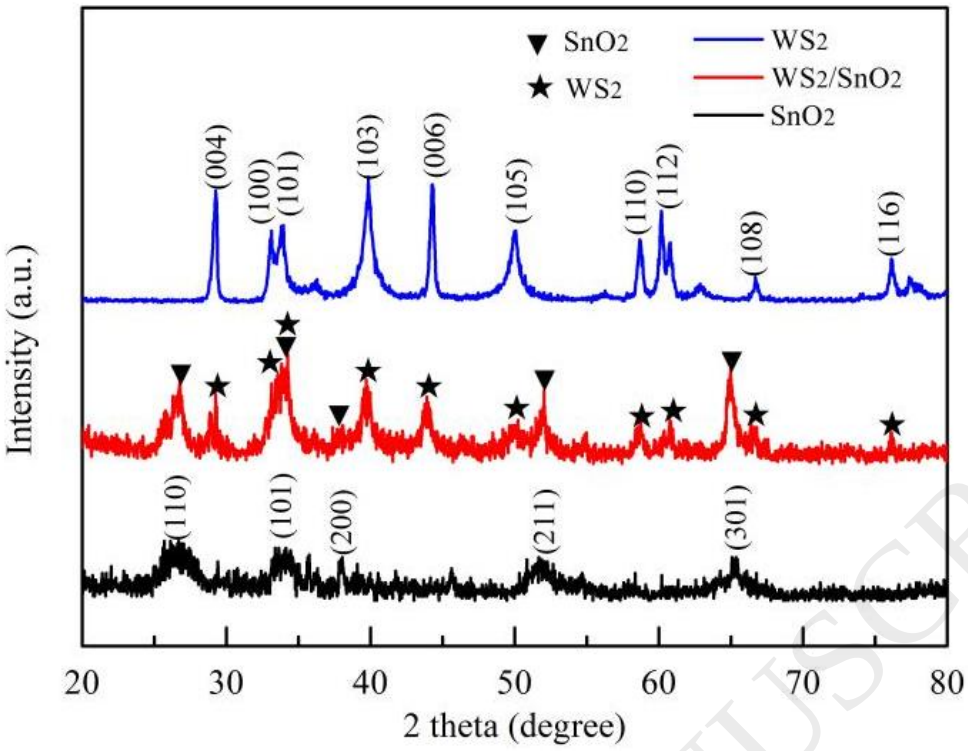

Figure 3. XRD of WS_2, SnO_2, and WS_2/SnO_2 samples.

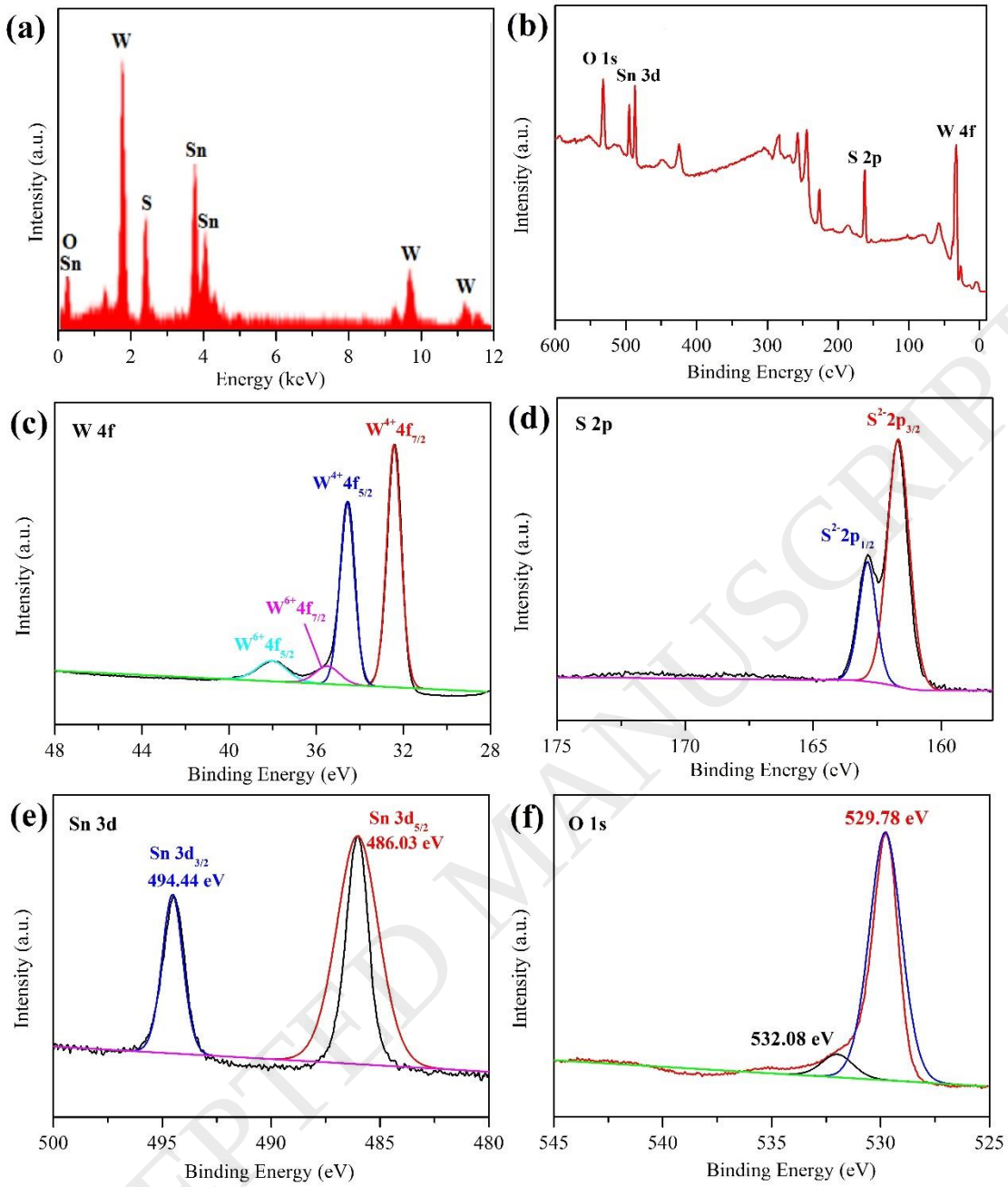

Figure 4. (a) EDS for WS_2/SnO_2 nanocomposite. XPS spectra of WS_2/SnO_2 sample: (b) survey spectrum, (c) W spectrum of WS_2/SnO_2 sample, (d) S spectrum of WS_2/SnO_2 sample, (e) Sn spectrum of WS_2/SnO_2 sample, and (f) O spectrum of WS_2/SnO_2 sample.

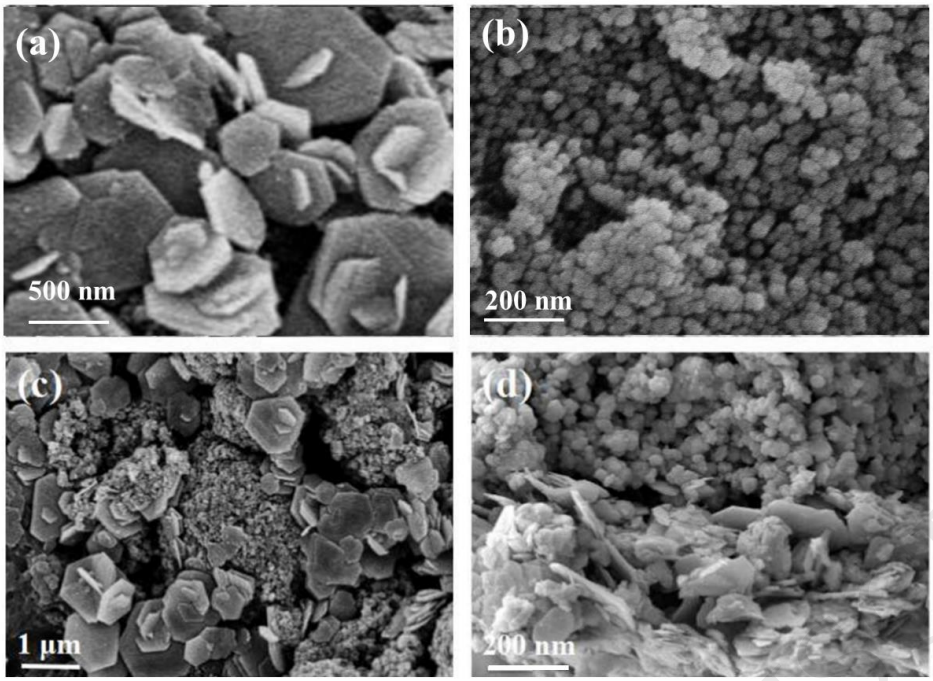

Figure 5. SEM images of (a) hexagonal WS_2 sample, (b) SnO_2 sample and (c) WS_2/SnO_2 nanocomposite, (d) cross-sectional images of WS_2/SnO_2 film.

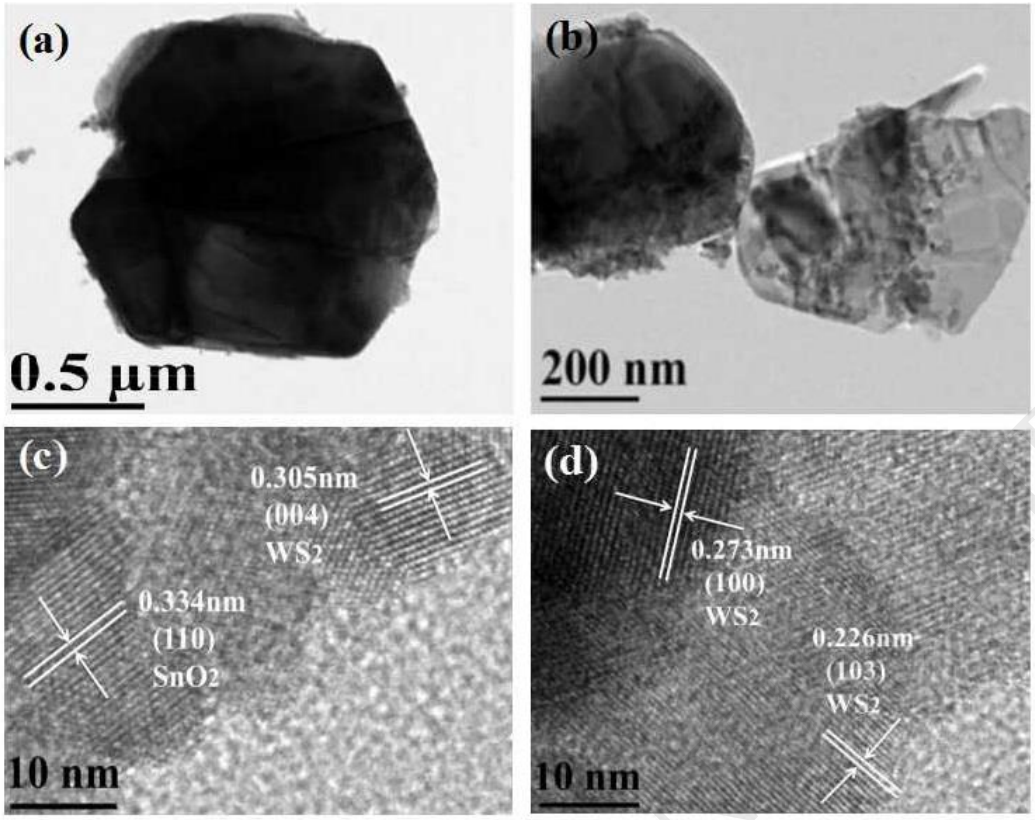

Figure 6. TEM images of (a) WS_2 microsheets and (b) WS_2/SnO_2 nanocomposite. HRTEM images of (c) WS_2/SnO_2 nanocomposite and (d) WS_2 microsheets.

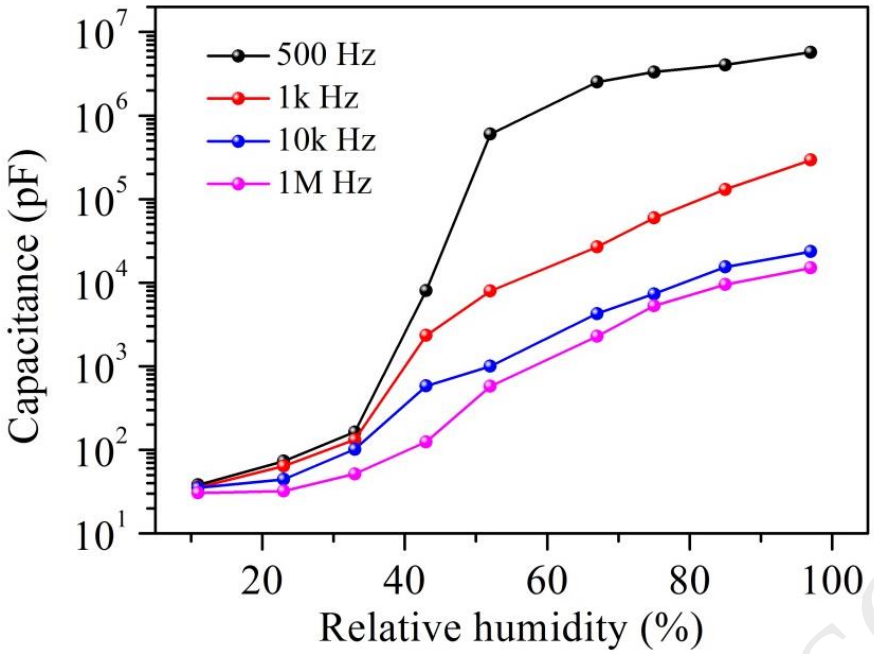

Figure 7. The capacitance of WS_2/SnO_2 film sensor exposed to various RH levels with different operation frequencies.

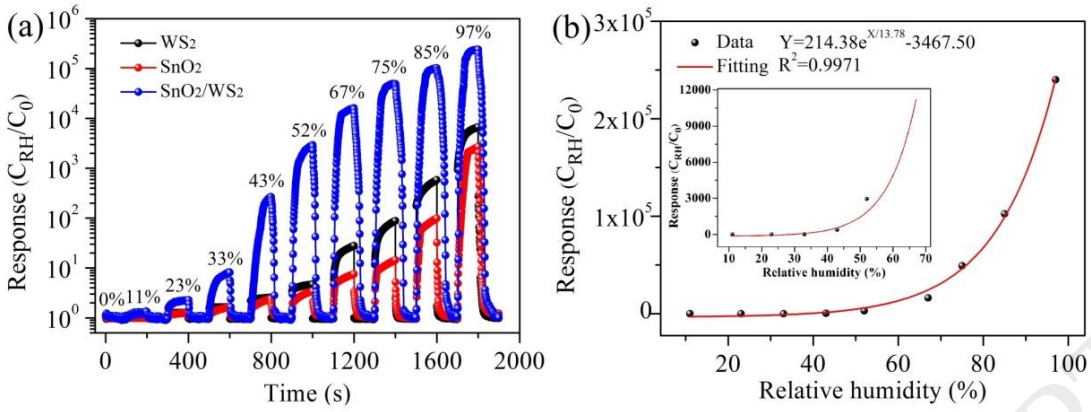

Figure 8. (a) Comparative results of WS_2/SnO_2 film sensor in sensing response with pure WS_2, and pure SnO_2 film. (b) The response of WS_2/SnO_2 film sensor as a function of RH in the range of 11−97%. Inset: the sensor response toward 11−67% RH.

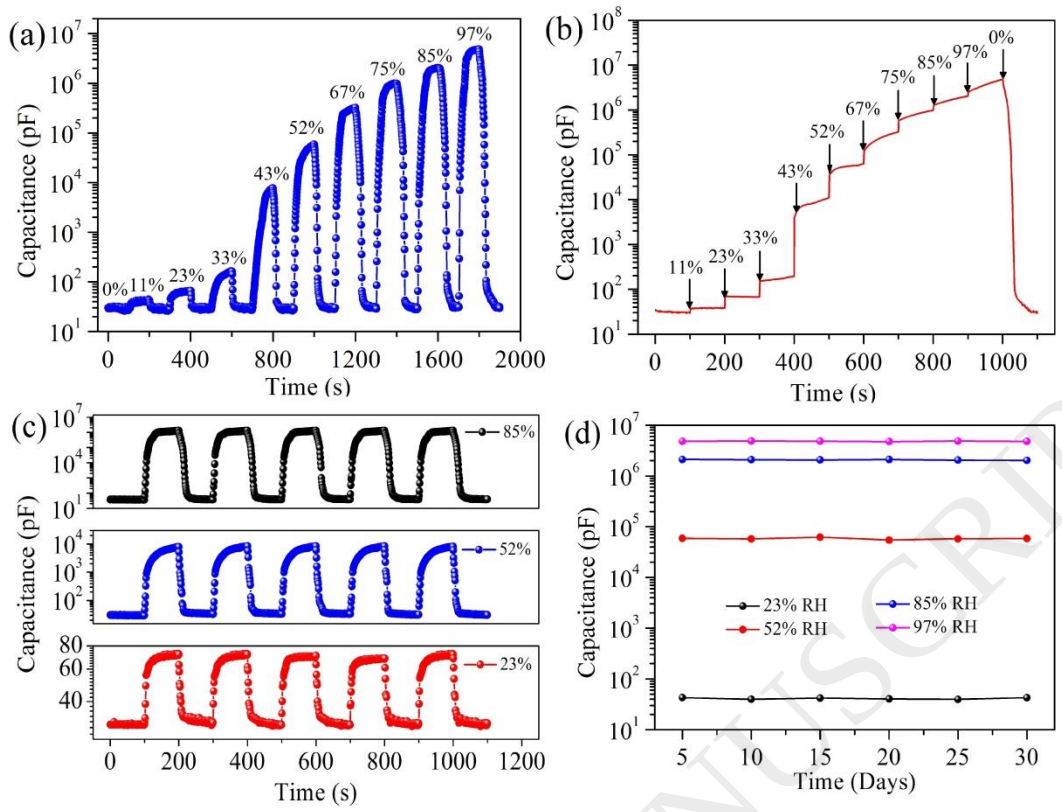

Figure 9. Sensing characteristics of LbL self-assembled WS_2/SnO_2 film sensor. (a) Time-dependent capacitance measurement toward switching RH. (b) Capacitance response toward step increases of RH and then recovery. (c) Repeatability performance exposed to 23%, 52%, and 85%RH. (d) Long-term stability exposed to 23%, 52%, 85% and 97%RH.

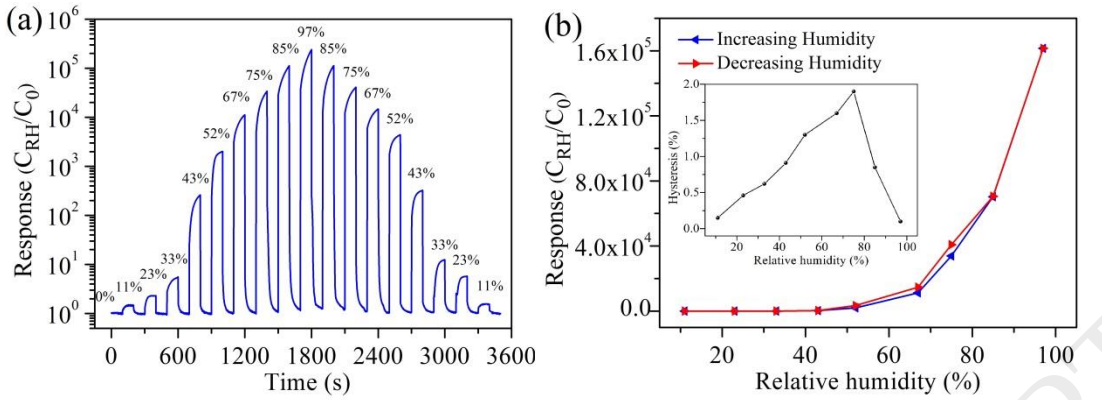

Figure 10. (a) The response and recovery characteristics under humidity cycling of absorption and desorption toward different RH. (b) Hysteresis loop characteristics of the WS_2/SnO_2 film sensor. Inset: hysteresis under different RH.

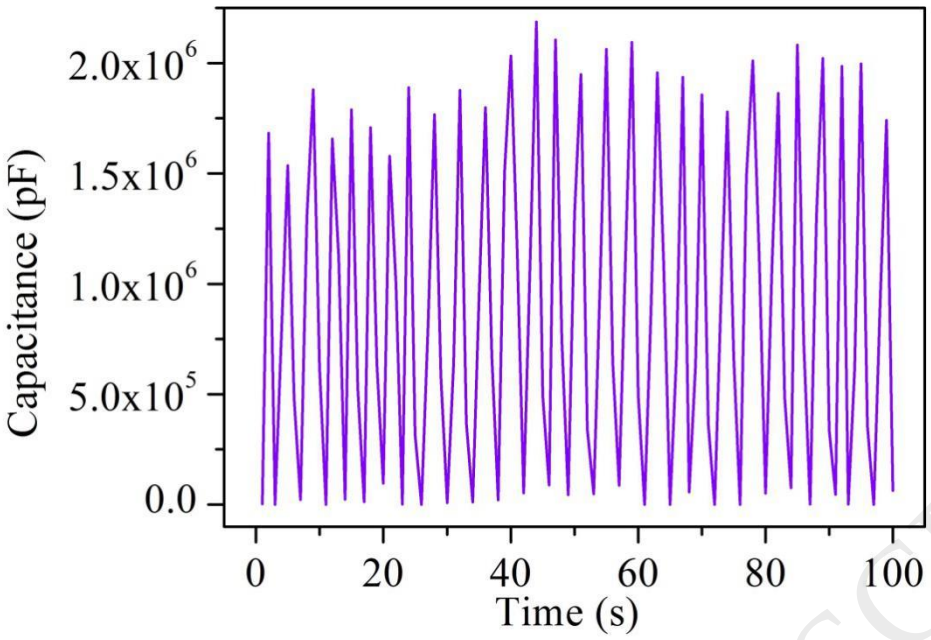

Figure 11. Capacitance response of the sensor toward human respiration.

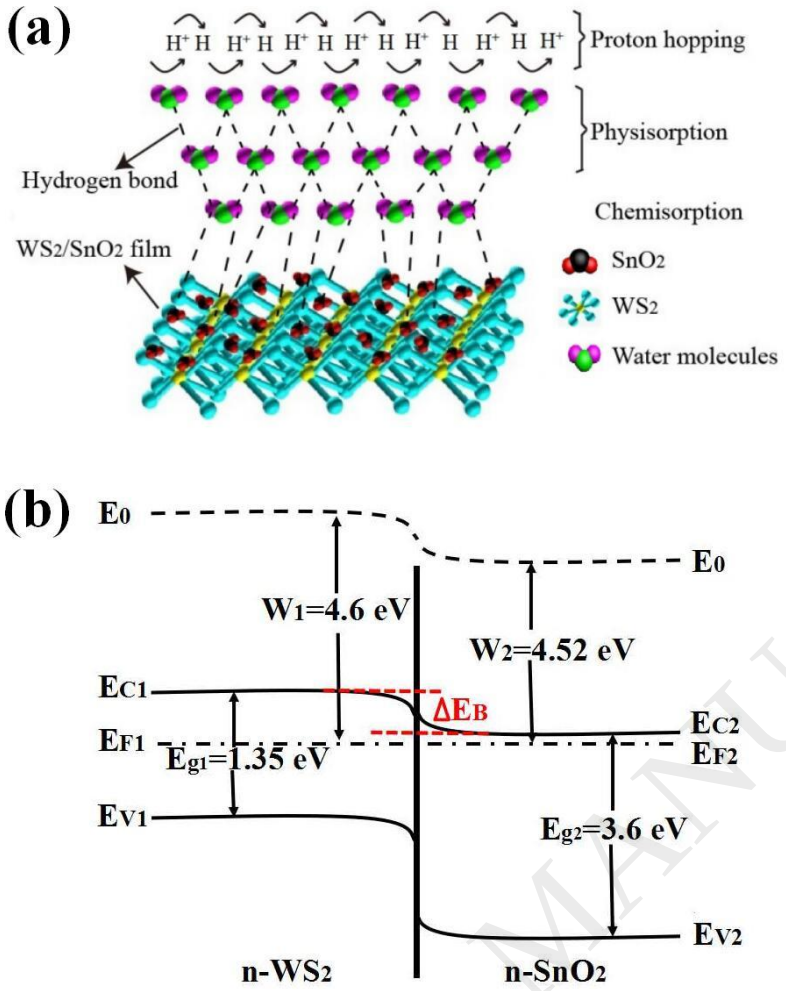

Figure 12. (a) Schematic of humidity sensing at WS_2/SnO_2 nanocomposite film. (b) Energy-band diagram of WS_2/SnO_2 film (E_0, vacuum-energy level; W, work function; E_g, energy band gap; E_F, Fermi level; E_C, conduction band; E_V, valence band).

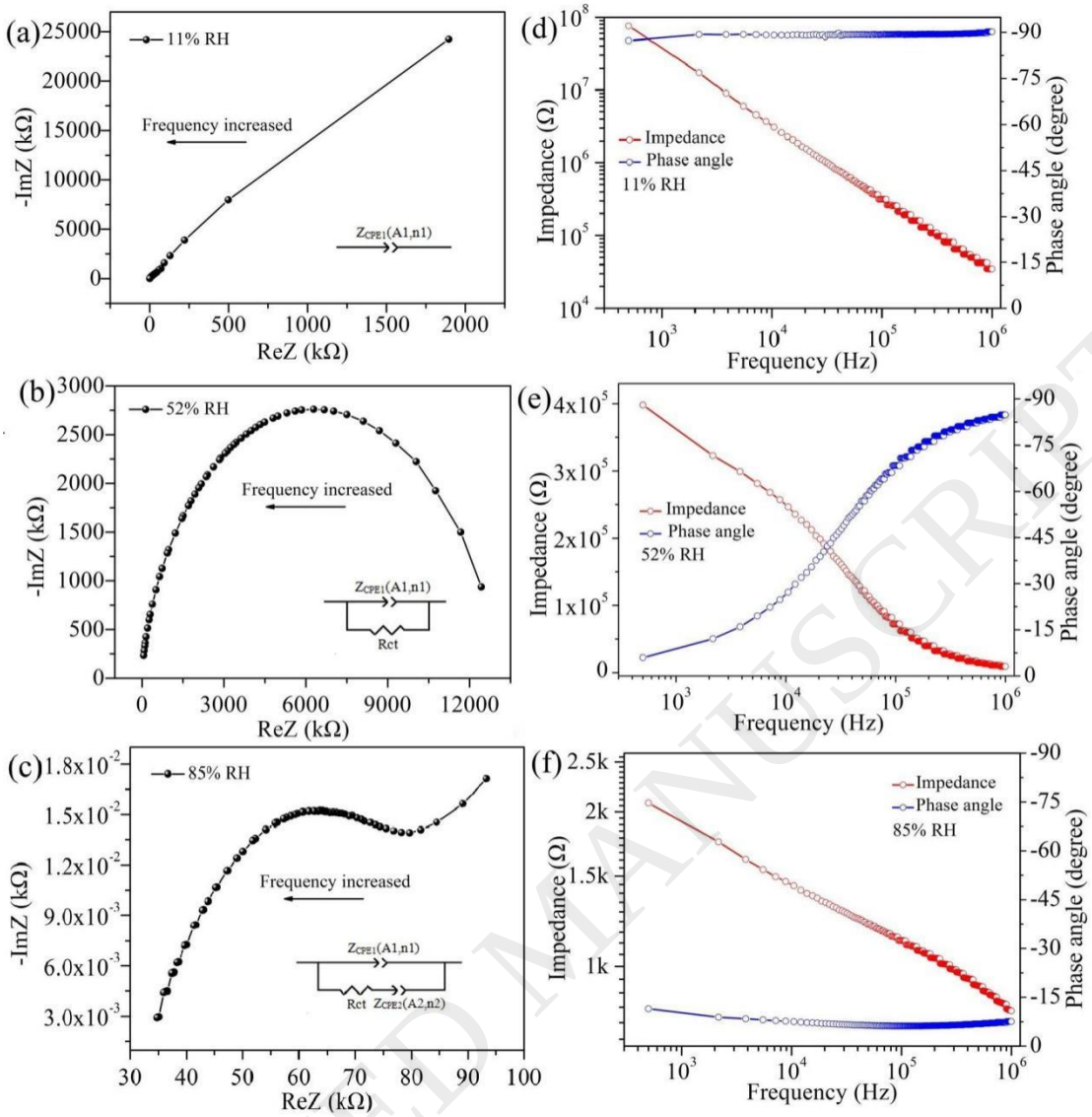

Figure 13. Complex impedance spectra, equivalent circuits (a, b, c) and corresponding Bode plots (d, e, f) of WS_2/SnO_2 film at different RH: (a and d) 11% RH, (b and e) 52% RH, and (c and f) 85% RH.

Table 1. Humidity sensing properties in this work compared with previous work.

Sensor materials	Fabrication method	Measuring range	Response	Sensitivity	Ref.
Graphene/SnO_2	Hydrothermal	11−97%RH	560.85	1604.89 pF/%RH	[11]
Graphene oxide (GO)	Solution dripping	15−95%RH	378	46.253 pF/%RH	[52]
WS_2	Sulfurization	20−90%RH	2357	−	[53]
WS_2	Liquid exfoliation	40−80%RH	37.5	−	[54]
MoS_2	Hydrothermal	17.2−89.5%RH	67.34	81.9 pF/%RH	[55]
GO/polyelectrolyte	LbL self-assembly	11−97%RH	2656.4	1552.3 pF/%RH	[56]
MoS_2/Ag	Solution dripping	11−97%RH	1729.25	21112 pF/%RH	[57]
WS_2/SnO_2	LbL self-assembly	11−97%RH	141260	55846 pF/%RH	This work